Published in final edited form as:
Neuron. 2010 July 15; 67(1): 49–60. doi:10.1016/j.neuron.2010.05.023.

Melanopsin-expressing retinal ganglion-cell photoreceptors: cellular diversity and role in pattern vision

Jennifer L. Ecker[1], **Olivia N. Dumitrescu**[3], **Kwoon Y. Wong**[3], **Nazia M. Alam**[4], **Shih-Kuo Chen**[1], **Tara LeGates**[1], **Jordan M. Renna**[3], **Glen T. Prusky**[4], **David M. Berson**[3], and **Samer Hattar**[1,2,*]

[1] Department of Biology, Johns Hopkins University, Baltimore, MD 21218, USA

[2] Department of Neuroscience, Johns Hopkins University, Baltimore, MD 21218, USA

[3] Department of Neuroscience, Brown University, Providence, RI 02912, USA

[4] Department of Physiology and Biophysics, Weill Cornell Medical College, Burke Medical Research Institute, White Plains, NY 10605, USA

Abstract

Using the photopigment melanopsin, intrinsically photosensitive retinal ganglion cells (ipRGCs) respond directly to light to drive circadian clock resetting and pupillary constriction. We now report that ipRGCs are more abundant and diverse than previously appreciated, project more widely within the brain, and can support spatial visual perception. A Cre-based melanopsin reporter mouse line revealed at least five subtypes of ipRGCs with distinct morphological and physiological characteristics. Collectively, these cells project beyond the known brain targets of ipRGCs to heavily innervate the superior colliculus and dorsal lateral geniculate nucleus, retinotopically-organized nuclei mediating object localization and discrimination. Mice lacking classical rod-cone photoreception, and thus entirely dependent on melanopsin for light detection, were able to discriminate grating stimuli from equiluminant gray, and had measurable visual acuity. Thus, non-classical retinal photoreception occurs within diverse cell types, and influences circuits and functions encompassing luminance as well as spatial information.

Keywords

ipRGCs; melanopsin; retinal ganglion cells; SCN; OPN; pupillary light response; circadian photoentrainment; visual water task; optokinetic tracking

Introduction

A small percentage of mammalian retinal ganglion cells contain the photopigment melanopsin and are capable of autonomous phototransduction (Berson et al., 2002; Hattar et al., 2002; Provencio et al., 2000; Provencio et al., 2002). These intrinsically photosensitive retinal ganglion cells (ipRGCs) combine their direct, melanopsin-based photoresponses with signals derived from rods and cones, and convey these directly to a subset of retinal targets

*Editorial correspondence: Dr. Samer Hattar, Assistant Professor, Johns Hopkins University, Department of Biology, 3400 N. Charles Street/Mudd 227, Baltimore, MD 21218, Tel: 410-516-4231, fax: 410-516-5213, shattar@jhu.edu.

in the brain. The ipRGCs mediate a variety of physiological responses to ambient light, such as circadian photoentrainment and the pupillary light reflex (Guler et al., 2008; Hatori et al., 2008; Lucas et al., 2003; Panda et al., 2002; Ruby et al., 2002).

Melanopsin-expressing ipRGCs were previously considered to be a homogenous cell population, with sparsely branched dendritic arbors stratifying in the outermost sublamina of the inner plexiform layer (IPL) (Berson et al., 2002; Hattar et al., 2002; Provencio et al., 2002). Subsequent work revealed morphological and functional diversity among ganglion cells expressing melanopsin or exhibiting intrinsic photosensitivity (Baver et al., 2008; Dacey et al., 2005; Sekaran et al., 2003; Tu et al., 2005; Viney et al., 2007). A second type of melanopsin-expressing ipRGCs has a monostratified dendritic arbor in the inner part of the IPL. First discovered in primate retina (Dacey et al., 2005), these cells have also been observed in rodents, where they are termed M2 or Type II cells to distinguish them from the originally characterized, outer-stratifying M1 or Type I cells (Baver et al., 2008; Hattar et al., 2006; Provencio et al., 2002; Schmidt and Kofuji, 2009; Viney et al., 2007). Indirect evidence suggests that M2 ipRGCs share some central targets with M1 cells, including the suprachiasmatic nucleus (SCN) and olivary pretectal nucleus (OPN) (Baver et al., 2008; Guler et al., 2008; Hattar et al., 2006). Other variants of ipRGCs have been reported, some with cell bodies displaced to the inner nuclear layer and others with bistratified dendritic arbors (sometimes called “Type III cells” and will be referred to as M3 cells) (Hattar et al., 2002; Provencio et al., 2002; Schmidt and Kofuji, 2009; Schmidt et al., 2008; Viney et al., 2007). The photosensitivity and brain projections of these newer cell types are less well characterized than those of M1 ipRGCs. The identification of new subtypes of melanopsin cells raises the prospect that the ipRGC retinal diversity extends to new innervation of brain targets for supporting other light-dependent physiological functions.

Results

To characterize the diversity of melanopsin cells in morphology, electrophysiology and brain targets, we made knock-in mice (*Opn4*^{Cre}) that express the Cre recombinase in place of the melanopsin (*Opn4*) open reading frame (Fig. S1A and B). The *Opn4*^{Cre} system allows the manipulation of loxP-flanked target genes selectively in melanopsin-expressing cells (Hatori et al., 2008). To visualize cells that express the CRE protein, we mated *Opn4*^{Cre} mice to one of two Cre-dependent reporter lines that use the same strong promoter (β-actin promoter and CMV enhancer; CAG) to drive the reporter gene expression (Fig. S1C and D). Cre-mediated recombination triggers expression of placental alkaline phosphatase in one of these lines (Z/AP; (Lobe et al., 1999)) and expression of enhanced green fluorescent protein (EGFP) in the other line (Z/EG; (Novak et al., 2000)). In both reporter lines, a small percentage of ganglion cells was labeled with the reporter protein (Fig. 1A and B) and labeled dendrites arborized both in the inner and outer sublaminae of the IPL (Fig. 1A), as expected from the laminar distribution of melanopsin protein (Provencio et al., 2002). Since similar knock-in strategies have successfully expressed several transgenes in ipRGCs (Guler et al., 2008; Hattar et al., 2002), it is not surprising that the majority of melanopsin-immunoreactive cells expressed the reporter proteins, indicating that the reporter line consistently identifies melanopsin-expressing cells (Fig. 1C–H). However, many ganglion cells lacking melanopsin immunoreactivity also expressed the marker, as observed in a previous publication using another Opn4^{Cre} line (Hatori et al., 2008). The total number of cells expressing the reporter proteins greatly exceeded prior estimates of melanopsin-expressing neurons. For example, in *Opn4*$^{Cre/+}$*; Z/AP* mice, we counted 2058 ± 141 cells per retina (n = 4), two to three times more cells than exhibit anti-melanopsin immunostaining (Lin et al., 2008; Robinson and Madison, 2004) or by expression of a tau-LacZ reporter gene from the melanopsin locus (Hattar et al., 2006; Hattar et al., 2002).

Whole-cell patch-clamp recordings of EGFP-positive ganglion cells in *Opn4$^{Cre/+}$; Z/EG* mice, in the presence of synaptic blockers, revealed that nearly all (46 of 51 cells tested; 90%) were intrinsically photosensitive (Fig. 2, and Fig. S2), even when they lacked detectable melanopsin immunoreactivity (Fig. 2H and I). Under pharmacological blockade of retinal synapses, these cells exhibited sluggish, persistent light responses, characteristic of melanopsin-based phototransduction (Wong et al., 2005;Wong et al., 2007). A small minority of EGFP-labeled cells lacked demonstrable intrinsic photosensitivity (5 of 51 cells; 10%), but exhibited brisk synaptically driven light responses (data not shown). Such cells may have either leaky expression or may have transiently expressed melanopsin during development; this would have triggered permanent expression of the marker proteins, since after Cre-mediated excision of the stop codon, marker protein expression is regulated solely by the promoter of the reporter transgene (Fig. S1C and D).

We also detected the marker proteins in a small percentage of rods and cones; these were melanopsin immunonegative (Fig. 1C–H). Their labeling by the marker proteins could be due either to leaky or transient expression of Cre or because the Cre system is more sensitive than immunohistochemistry for detecting melanopsin expression. The finding may be linked to melanopsin-like immunoreactivity in a very few human cones (Dkhissi-Benyahya et al., 2006).

We used dye filling to visualize the morphology of the reporter-labeled cells that were intrinsically photosensitive. Labeled cells included not only the previously characterized M1 and M2 ipRGCs, but also several new morphologically distinct ganglion cell types (Fig. 2 and Fig. S2). M1 ipRGCs had sparsely branching monostratified dendritic ramifications in the outermost IPL, had an average dendritic field diameter of 350 ± 87 μm (mean ± s.d.; n=12) and cell body diameter of 15.6 ± 2.4 μm (n = 7; Fig. 2A). M2 ipRGCs had relatively large radiate dendritic arbors (Fig. 2B) stratifying within the inner half of the IPL (ON sublayer). Dendritic field diameters (324 ± 30 μm; mean ± s.d.; n = 4) were similar in size to those of M1 ipRGCs, but the arbors were more orderly, with more regular branching angles and more uniform dendritic density within the field (Fig. 3A). The cell bodies of M2 ipRGCs were slightly larger on average than those of M1 cells (17.4 ± 1.7 μm; n = 5). All M1 and M2 ipRGCs tested were melanopsin immunopositive (Fig. 2D, E, F and G; n = 15 M1 and 11 M2). Though both subtypes invariably exhibited an intrinsic light response (Fig. 2J and K), the response in M1 ipRGCs was an order of magnitude larger than that of the M2 ipRGCs with a shorter latency to peak (Fig. 2J, and Fig. S3A and B), confirming an earlier report (Schmidt and Kofuji, 2009).

We encountered at least two additional subtypes of intrinsically photosensitive cells among the EGFP-positive ganglion cells that were melanopsin immunonegative (Fig. 2H, I and Fig. S2; data not shown). One type resembled an ON alpha ganglion cell (Fig. 2C, n=6), with a large soma (17.1–22.3 μm diameter; n = 3) and a large radiate dendritic arbor (302–444 μm diameter; n = 3) monostratifying in the ON sublayer. These cells exhibited weak intrinsic light responses (Fig. 2L; peak photocurrent of 18.5 ± 11.4 pA; n = 4). We provisionally term these alpha-like cells “M4,” (reserving “M3” for the bistratified ipRGCs). The second type of EGFP-positive but melanopsin-immunonegative ipRGC also stratified in the ON sublayer of the IPL, but could be distinguished from both M2 and alpha-like M4 ipRGCs by its relatively compact, highly branched dendritic arbor (Fig. S2A; diameter: 149–217 μm; n = 3). Of the eight cells of this group that were tested, seven were intrinsically photosensitive, although as with the M2 and M4 ipRGCs, these responses were much weaker (peak photocurrents 12.9 ± 4 pA, Fig. S2B) than those of M1 ipRGCs. We provisionally term these smaller-field bushy type neurons “M5 cells.”

The M2 and M4 ipRGCs are the least readily distinguished, because both have large radiate dendritic arbors stratifying in the ON sublayer. To clarify the morphological distinctions between them, we filled dozens of EGFP-positive RGCs by intracellular dye injection with a sharp electrode, which preserves the morphology of the ipRGCs. We reconstructed the somadendritic profiles of all well-filled cells with wide-field dendritic arbors limited to the inner IPL (thus excluding M1, M3 (bistratified), and M5 cells). Dye filled cells could be readily divided into M2 and M4 subtypes (Fig. 3). Drawings of representative examples show that M2 cells had dendritic arbors that were sparser and slightly smaller than those of M4 cells (Fig. 3). By comparison with M4 cells, M2 cells had fewer branchpoints (Fig. 3C), less total dendritic length (Fig. 3B), and a smaller dendritic-field diameters (Fig. 3C). Their axons also appeared consistently finer than those of M4 cells. We encountered three additional EGFP-positive cells that were intrinsically photosensitive, but lacked detectable melanopsin immunoreactivity. These were not easily grouped with any of the subtypes described above; all had relatively weak intrinsic light responses (<20 pA) and bushy, highly branched dendrites. Our failure to detect melanopsin in the M4 and M5 ipRGCs is presumably because their expression of the pigment is very low and because both the Cre labeling system and electrophysiological recordings of photoresponses detect it with greater sensitivity than does immunofluorescence.

All of the ipRGC cell types also exhibited synaptically mediated excitatory influences from rods and/or cones, as reflected by brisk light responses from M2 and M4 subtypes that were abolished by blockade of ionotropic and metabotropic glutamate receptors (Fig. S3C–F).

In order to trace the axons of the new types of melanopsin cells to their brain targets, we used the *Opn4*$^{Cre/+}$*; Z/AP* mouse, which uses the same promoter as the Z/EG line (Fig. S1C and D). Placental alkaline phosphatase (AP) is expressed in the plasma membrane of tagged cells, including their axons, where it can be visualized by histochemical staining. In the retina, the AP staining was similar to that observed with EGFP labeling in the *Opn4*$^{Cre/+}$*; Z/EG* (Fig. 1), with similar cell numbers and morphological subtypes. We examined the distribution of AP-positive axons in the brain to obtain an overview of the central projections of all ipRGCs. Labeled axons were evident in the optic nerve, chiasm and tract as well as in a number of central visual nuclei (Fig. 4A–E). Before attributing all such axonal labeling to retinofugal fibers, however, we had to consider non-retinal sources, since AP was expressed in a limited number of neurons distributed in the cerebral cortex, diencephalon and brainstem (Fig. S4F, and G). We examined brain sections from mice in which both eyes had been removed three weeks earlier, sufficient time to ensure virtually complete degeneration of retinofugal axons (Fig. S4). Essentially no AP staining remained within the retinorecipient nuclei in these animals (Fig. S4A–E), whereas cellular and axonal labeling persisted in most non-visual areas (Fig. S4F, and G). Therefore, all fiber labeling within visual nuclei arises from AP-positive retinal ganglion cells.

Labeled retinofugal fibers terminated in all of the previously established targets of melanopsin-expressing RGCs (Baver et al., 2008; Gooley et al., 2001; Hannibal and Fahrenkrug, 2004; Hattar et al., 2006; Hattar et al., 2002; Sollars et al., 2003), including the SCN (Fig. 4A, left), the intergeniculate leaflet and ventral division of the dorsal lateral geniculate nucleus (dLGN; Fig. 4B, left and Fig. 5), and the OPN (Fig. 4C, left). The most comprehensive prior description of the projections of melanopsin-expressing RGCs was based on a reporter mouse (*Opn4*$^{tau\text{-}LacZ}$) in which a gene coding for the tau signal peptide fused to β-galactosidase was targeted to the melanopsin (*Opn4*) gene locus (Hattar et al., 2006; Hattar et al., 2002)(Fig. 4A–E, right). Available evidence indicates that the X-gal staining in this mouse selectively labels M1 melanopsin cells (Baver et al., 2008; Hattar et al., 2006). In contrast, at least five ganglion-cell types express AP in the *Opn4*$^{Cre/+}$*; Z/AP* line by virtue of melanopsin-driven Cre-mediated recombination including displaced and

bistratified ipRGCs. Comparing labeled fiber distributions between the *Opn4*$^{tau\text{-}LacZ/+}$ and *Opn4*$^{Cre/+}$*; Z/AP* thus provide important clues to the central targets of non-M1 melanopsin cells. Therefore, we stained coronal brain sections from *Opn4*$^{tau\text{-}LacZ/+}$ and *Opn4*$^{Cre/+}$*; Z/AP* and compared the distribution of axons labeled by the reporter proteins in several retinorecipient nuclei of the brain (Fig. 4A–E). With the more sensitive Cre-dependent AP labeling, we find much more extensive axonal labeling in the dLGN (especially ventromedially; Fig. 5), the core of the OPN, the posterior pretectal nucleus, and the superior colliculus (SC) than that of LacZ line (Hattar et al., 2006; Hattar et al., 2002) (Fig. 4B–E). The accessory optic system was devoid of labeling. Further details about these projections are provided in Supplemental Text.

We next generated a mouse permitting direct comparison of the axonal projections of the subset of melanopsin-expressing ganglion cells (predominantly M1 ipRGCs) labeled in the *Opn4*$^{tau\text{-}LacZ}$ mouse (Hattar et al., 2006; Hattar et al., 2002) with those of the expanded set of melanopsin-expressing cell types labeled by the cre-lox system. For this purpose, the Z/AP transgene was unsuitable for reporting Cre expression (i.e., *Opn4*$^{Cre/tau\text{-}LacZ}$*; Z/AP*) because its lacZ cassette (Fig. S1C) yields β-galactosidase expression in all cells not expressing CRE, and this would mask the β-galactosidase reporter in ipRGC axons. We therefore used Brainbow-1.0 mice (Livet et al., 2007) to generate *Opn4*$^{Cre/tau\text{-}lacZ}$*; Brainbow-1.0* animals, in which Cre-mediated recombination yields expression of fluorescent proteins (FPs) under the control of the Thy-1 promoter selectively in melanopsin-expressing cells (Fig. S1E). In these animals, retinas expressed the Cre-reporting FPs in most of the ganglion cells that expressed β-galactosidase (M1 ipRGCs) but in a larger number of other ganglion cells as well (Fig. 6A). Likewise, many labeled axons in the brain were immunopositive for FPs but not for β-galactosidase, and these arise from ipRGCs that are non-M1 ipRGCs. In agreement with Figure 4, axons labeled with the FPs constituted the overwhelming majority of labeled retinal afferents in certain nuclei, including the dLGN and parts of the vLGN (Fig. 6C), the core of the OPN (Fig. 6B), the posterior pretectal nucleus and the superior colliculus. In several of the known targets of M1 ipRGCs, such as the SCN, IGL, and subregions of the vLGN, double labeled (FP- and β-gal positive) fibers were intermixed with axons labeled only with FPs (Fig. 6C and D). This implies convergent inputs to these nuclei from M1 and non-M1 ipRGCs, as anticipated for the SCN from the findings of Baver et al. (2008). Finally, in several target structures (OPN shell (Fig. 6B) and habenular region (not shown)), virtually all axons were double labeled, suggesting that M1 ipRGCs were the only type of melanopsin-expressing ganglion cell to innervate these nuclei. FP immunoreactivity was weak in the fibers projecting to the OPN shell (Fig. 6B), perhaps due to low expression of Thy-1 in these M1 ipRGCs.

The extensive projections of reporter-labeled axons to the dLGN and SC are surprising because these nuclei mediate spatial and discriminative visual functions very different from the non-image-forming mechanisms to which ipRGCs are traditionally linked. This prompted us to examine whether melanopsin-based phototransduction might support pattern vision in the absence of functioning rods and cones. In the Visual Water Task (Prusky et al., 2000), we assessed the visual performance of a mouse strain in which rod and cone phototransductions are silenced (Hattar et al., 2003), leaving ipRGCs as the only functional photoreceptors (*Gnat1*$^{-/-}$*; Cnga3*$^{-/-}$ double knockout animals; (Altimus et al., 2008)). The *Gnat1*$^{-/-}$ *Cnga3*$^{-/-}$ double knockout animals and WT animals have similar melanopsin expression in the retina as revealed by immunohistochemistry (Fig. S5A) and real time quantitative PCR (qPCR; Fig. S5B). *Gnat1*$^{-/-}$, is a rod transducin knockout line that eliminates rod phototransduction (Calvert et al., 2000), whereas *Cnga3*$^{-/-}$ line eliminates the cone cyclic nucleotide gated channel causing the absence of cone phototransduction (Biel et al., 1999). *Gnat1*$^{-/-}$*; Cnga3*$^{-/-}$ mice in the absence of the melanopsin protein (triple knockout animals; *Gnat1*$^{-/-}$*; Cnga3*$^{-/-}$*; Opn4*$^{-/-}$) lack circadian photoentrainment,

sustained pupillary light reflex or direct light effects (masking responses) on wheel running activity (Hattar et al., 2003). *Gnat1*$^{-/-}$*; Cnga3*$^{-/-}$ mice, which contain only ipRGCs as functional photoreceptors, were indeed able to discriminate high-contrast, sinusoidally-modulated gratings from uniform gray stimuli of the same mean luminance, although they needed roughly twice as many trials as control mice to reach criterion performance (70% correct, measured at 0.12 cycles/degree (c/d); Fig. 7D). The acuity in the *Gnat1*$^{-/-}$*; Cnga3*$^{-/-}$ mice was measurable at 0.16 ± 0.002 c/d (mean ± std. error) (Fig. 7C, E), though it was much lower than that of wildtype animals (C57/Bl6; 0.55 ± 0.006 c/d). In addition, using cfos immunostaining in the visual cortex, we show that *Gnat1*$^{-/-}$*; Cnga3*$^{-/-}$ mice have higher cfos expression in the cortex when they are exposed to a pattern (Fig. 8A and B).

If the residual pattern vision in mice lacking functional rods and cones was mediated by melanopsin, it should be abolished by the additional deletion of melanopsin in this rod/cone functional knockout background (triple knockouts *Gnat1*$^{-/-}$*; Cnga3*$^{-/-}$*; Opn4*$^{-/-}$; (Hattar et al., 2003)). Indeed, *Gnat1*$^{-/-}$*; Cnga3*$^{-/-}$*; Opn4*$^{-/-}$ mice were unable to reach criterion performance at 0.12 c/d, even after 405 trials (Fig. 7C and D) and failed to show any cfos staining in the cortex (Fig. 8A and B). Surprisingly, the triple knockout animals (like *Gnat1*$^{-/-}$*; Cnga3*$^{-/-}$ and wildtype mice) were able to discriminate between two uniform stimuli differing markedly in luminance. In triple knockout animals, this ability may be traceable to the early receptor potential of rods and cones, a very small, transient hyperpolarization caused by charge movements triggered when light causes conformational changes in a large numbers of photopigments molecules in rod outer segments (Cone, 1967; Woodruff et al., 2004). This mechanism has been proposed to explain the very weak pupillary light reflex in some of the triple knockout animals (Guler et al., 2007; Hattar et al., 2003).

In optokinetic tracking (OKT; (Prusky et al., 2004)), a measure of reflexive retinal image stabilization, *Gnat1*$^{-/-}$*; Cnga3*$^{-/-}$ animals (with ipRGCs as the only functional photoreceptors) performed no better than the triple knockout animals; neither strain tracked the drifting grating, whereas wildtype animals showed a spatial frequency of 0.39 ± 0.001 c/d (Fig. 7A). The ability of *Gnat1*$^{-/-}$*; Cnga3*$^{-/-}$ animals to perform spatial visual discriminations, but not to optokinetically track gratings, is consistent with the axonal projections of reporter-labeled RGCs and provides additional evidence that rods and cones are not functional in these animals. The terminations of ipRGCs occur within the dLGN and SC, structures associated with visual perceptual function, but they do not innervate the accessory optic nuclei, which mediate reflexive retinal image stabilization (Douglas et al., 2005). Together, these results indicate that melanopsin-based phototransduction supports pattern vision in the absence of functioning rod and cone photoreceptors.

Discussion

Our findings indicate that melanopsin-based inner retinal photoreception is more widespread and diverse than previously appreciated, involving more ganglion cell subtypes, novel central targets, and broader functional roles. We find at least five subtypes of ipRGCs in the mouse retina. Collectively, these ipRGCs project to a wider array of visual nuclei than originally identified using the *Opn4*$^{tau\text{-}LacZ}$ reporter line (Hattar et al., 2006). Of particular interest are the much more extensive projections to the SC and the dLGN. Both of these nuclei are retinotopically organized and have been implicated in spatial vision rather than in the non-image-forming photic behaviors with which ipRGCs have been traditionally thought to influence. Our behavioral findings demonstrate that mice lacking functional rods and cones and thus reliant on ipRGCs for photoreception, possess discriminative spatial vision.

The great majority of retinal ganglion cells labeled in our Cre-based melanopsin reporter line are intrinsically photosensitive whether or not they are detectably melanopsin immunoreactive. Moreover, they exhibit light responses characteristic of melanopsin-based phototransduction, including sluggish onset and slow termination. Our inability to detect melanopsin by immunofluorescence in some of these cells indicates the superior sensitivity of the Cre system for identifying melanopsin-expressing ipRGCs. The strength of the photoresponses in EGFP-labeled cells appears to correlate with the level of melanopsin expression as revealed by immunohistochemistry, with the M1 ipRGCs exhibiting more intense immunolabeling and larger intrinsic light response than the other subtypes (see also (Schmidt and Kofuji, 2009)). Except for the M1 cells, all of the ipRGC types encountered stratified in the ON sublayer of the IPL. At least three varieties of such cells have been seen, distinguishable on the basis of dendritic field size and, to some extent, soma size. These include the M2 ipRGCs described by others (Baver et al., 2008; Hattar et al., 2006; Schmidt and Kofuji, 2009; Schmidt et al., 2008; Viney et al., 2007). We confirm that the intrinsic light response of M2 cells is similar in form but smaller in amplitude than that of M1 cells (Schmidt and Kofuji, 2009). An entirely new subtype of ipRGC revealed by the present study is a cell with large soma and wide, radiate dendritic arbor. These cells, which we term “M4,” are distinguishable from M2 cells by their more highly branched and slightly larger dendritic fields (Fig. 3), their coarser axons, and their lack of detectable melanopsin immunoreactivity. They resemble neurons observed in earlier surveys of mouse RGC morphology, and termed ON alpha, or RGA1 cells (Sun et al., 2002). They may also correspond to Cluster 10 (Coombs et al., 2007); Cluster 9 (Badea and Nathans, 2004), and either Cluster 11 or Cluster 8 (Kong et al., 2005). Finally, we also observed a smaller-field bushy type (“M5”) bearing some resemblance to the cells labeled Cluster 3-on (Coombs et al., 2007) and Clusters 4 or 5 (Kong et al., 2005). Both M4 and M5 cells have intrinsic light responses of relatively low amplitude, perhaps because they express melanopsin at low levels, as reflected in their lack of detectable melanopsin immunoreactivity. Further work is needed to learn to what extent these ipRGC types differ in stratification, sensitivity, phototransduction mechanisms, synaptic inputs or visual response properties.

Since the M4 subtype lacks melanopsin immunoreactivity, we wanted to address the concern that electrical coupling via gap junctions with other ipRGCs may drive the intrinsic light response in this subtype. Therefore, we have done experiments in which the gap-junction-permeant tracer Neurobiotin has been included in the pipette, and have seen no evidence for tracer coupling of other ganglion cell types. Indeed, in the extensive literature on tracer coupling in mammalian ganglion cells, there is no precedent for gap junctional contacts between RGCs belonging to different types (i.e., ‘heterotypic coupling’). The recent study of RGC coupling surveyed >20 types of RGC and found not one of them was heterotypically coupled to other RGC types (Volgyi et al., 2009). In addition, a recent publication showed weak but consistent anti-melanopsin immunostaining of large ganglion-cell somata (presumptive alpha-like cells) and in their proximal dendrites (Berson et al., 2010). This staining is abolished in melanopsin knockout animals. This pattern is entirely consistent with our suggestion that the M4 (alpha-like) cells express melanopsin at low levels that support weak intrinsic photosensitivity. We therefore judge it to be unlikely that the weak photosensitivity we observe in the ‘alpha-like’ M4 cells under blockade of chemical synapses is attributable to their gap-junctional coupling to melanopsin-expressing ipRGCs rather than to direct photosensitivity.

With respect to central projections, our findings suggest that these novel types of ipRGCs have a complex pattern of central distribution partially overlapping that of M1 ipRGCs, as inferred from the distribution of axonal β-galactosidase in the *Opn4*$^{tau\text{-}LacZ}$ mouse (Hattar et al., 2002; Hattar et al., 2006). In the SCN and IGL, both key nuclei in central circadian mechanisms, fibers from M1 and non-M1 ipRGCs appear intermixed. By contrast, M1

ipRGCs appear to constitute the predominant (if not the only) source of input to the habenular region and shell of the OPN, whereas non-M1 ipRGC axons greatly outnumber M1 afferents in the dLGN, SC, posterior pretectal nucleus, and core of the OPN.

The shell of the OPN appears to be the critical link between the retina and the pupillomotor output (Baver et al., 2008; Prichard et al., 2002). Thus the present data suggest that M1 ipRGCs may be the major, and possibly the sole source of retinal drive to the pupillary light reflex (Guler et al., 2008). The functional role of the inputs from non-M1 ipRGCs to the OPN core is unknown. They may contribute to pupillary function, for example, by contacting the dendrites of shell neurons extending into the core. Alternatively, the core could be largely distinct from the shell in its connections and functional roles.

The novel projections of melanopsin cells revealed here, and the persistence of pattern discrimination in mice in which ipRGCs are the only functional photoreceptors, provide the strongest evidence to date that the influences of ipRGCs extend well beyond the non-image-forming centers and homeostatic, reflexive responses to ambient light. Earlier reports have provided glimpses of such a broader role. Mice with virtually complete disruption of outer retinal photoreception, and thus reliant on melanopsin for photodetection, still exhibit a preference for dark environments and can use light as a cue to avoid shocks in a shuttle-box task (Mrosovsky and Hampton, 1997; Mrosovsky and Salmon, 2002). There has been evidence for projections from melanopsin expressing ganglion cells to the superior colliculus and dLGN (Dacey et al., 2005; Hattar et al., 2006; Morin et al., 2003), although these were very sparse in rodents (Hattar et al., 2006). The contribution to the geniculocortical pathway may provide a substrate for the luxotonic responses reported in some neurons of the striate cortex (Kayama et al., 1979). Recent findings in a human patient with a virtually complete loss of outer retinal function suggest that melanopsin-based photoresponses may support the conscious appreciation of light (Zaidi et al., 2007), although residual rod and cone function in this patient cannot be entirely excluded. The low grating acuity in mice in which ipRGCs are the only photoreceptors is in keeping with the low spatial density of ipRGCs relative to other ganglion cells and the large dendritic fields (and, thus presumably the receptive fields) of most of the ipRGCs identified here. The residual perceptual capacity in mice lacking functional rods and cones is probably attributable to the projections of ipRGCs to the dLGN, especially in light of cfos activation in the cortex; however, the ipRGC inputs to the superior colliculus and pretectum could also contribute. Wildtype mice retain the ability to discriminate patterns after ablations of the striate cortex, albeit with substantially reduced acuity (Prusky and Douglas, 2004), and this may involve parallel ascending visual pathways through the tectum, visual association nuclei of the thalamus, and extrastriate visual cortex. The superior colliculus also plays a key role in the orientation of gaze to visual cues, and it will be of interest in future studies to determine whether mammals lacking functional rods and cones may retain such orienting or other visuomotor reflexes.

Before ascribing the unexpected spatial vision in *Gnat1*$^{-/-}$*; Cnga3*$^{-/-}$ animals to novel types of ipRGCs, it is important to consider one other possible mechanism. We detected melanopsin-cre-driven reporter proteins in a minority of rods and cones. Were these cells capable of melanopsin-mediated phototransduction, they could activate conventional ganglion cells innervating the dLGN. We view this as unlikely because these rods and cones lack detectable melanopsin mRNA (Provencio et al., 2000) or melanopsin-like immunoreactivity (Fig. 1D and G). Moreover, melanopsin-based phototransduction in rods and cones would presumably drive all retinofugal pathways to some extent, and this is at odds with the complete absence of optokinetic tracking in these animals. By contrast, this absence of OKT in animals in which ipRGCs are the only functional photoreceptors is readily explained if phototransduction is restricted to ipRGCs, because these ganglion cells

lack any projection to the accessory optic system, an obligatory link between the retina and optokinetic system.

The extensive projection to the dLGN revealed here derives almost entirely from one or more of the inner-stratifying (non-M1) ipRGC types and terminates in a restricted ventromedial compartment of the nucleus strikingly similar to that innervated by a type of OFF alpha cell (Huberman et al., 2008). This compartment occupies the inner "core" region of the dLGN (Reese, 1988), including the zone of input from the ipsilateral eye. This adds to the growing body of evidence for laminar segregation of input from various types of ganglion cells innervating the murine dLGN (Hattar et al., 2006; Huberman et al., 2009; Quina et al., 2005), reminiscent of the more obvious and better characterized laminar specificity in other mammals.

Experimental Procedures

Animal models

All mice were of a mixed background (BL/6;129SvJ) and only Z/EG mice had a (BL/6;129SvJ;CD-1) background. Mice used in the electrophysiological studies were heterozygous for melanopsin (*Opn4*$^{Cre/+}$), aged 5.5 – 7 weeks, and those for histological examination were 2 – 4 months of age at the time of sacrifice. The detailed generation of all the animal models is provided in the supplementary experimental procedures. Animals that were used in the behavioral analysis were between 4–16 months. Animals were housed and treated in accordance with NIH and IACUC guidelines, and all animal care and use protocols were approved by the Johns Hopkins University, Brown University, and Weill Cornell Medical College Animal Care and Use Committees.

Enucleations

To remove both eyes, mice >2 months of age were first anesthetized intraperitoneally with 20 mL/kg Avertin. Fingers were placed on either side of the eye to allow it to bulge, and a curved pair of scissors was gently placed between the eye and the skin to cut the optic nerve. Bleeding was controlled by orbital pressure. The animal was monitored over the next several days for signs of infection. Tissue was harvested and processed 3 weeks following eye removal.

Alkaline phosphatase staining

Mice were deeply anesthetized with 30 mL/kg Avertin, then intracardially perfused with phosphate-buffered saline for 3 minutes followed by 40 mL of 4% paraformaldehyde. Retinas were isolated, mounted flat, and post-fixed for 30 minutes in 4% paraformaldehyde. Brains were removed and mounted in 3% agarose, then cut into 200 μm sections on a vibrating microtome (Vibratome 1000 Plus). Tissue was heat-inactivated for 90 – 120 minutes at 65°C. Alkaline phosphatase histochemistry was performed using NBT/BCIP tablets (Roche) for 2 – 4 hours in the dark with constant shaking. Tissue was washed three times with phosphate buffered saline containing 0.1% Tween-20 (Sigma-Aldrich), fixed 3 hours in 4% paraformaldehyde at 4°C, then dehydrated in an ethanol series. The following day, retinas and brain sections were cleared in a 2:1 mixture of benzyl benzoate:benzyl alcohol (Sigma-Aldrich), mounted in clearing solution, and imaged within two days.

Electrophysiology

Whole cell recordings were made in isolated, flat mounted retinas as previously described (Wong *et al.*, 2005; Wong *et al.*, 2007), obtained from animals 2–8 months of age. Cells expressing EGFP were located using brief exposure to blue epifluorescence excitation from a mercury lamp. Subsequent visual guidance of the patch electrode to the target cell was

thereafter conducted with infrared transillumination. To suppress the influence of rods and cones on the inner retina, thus revealing in isolation the intrinsic, melanopsin-driven light responses of ipRGCs (Wong *et al.*, 2005; Wong *et al.*, 2007), we bath-applied a cocktail of antagonists of metabotropic and ionotropic glutamate receptors. This included L-AP4 (L-(+)-2-amino-4-phosphonobutyric acid, a metabotropic glutamate receptor antagonist), AP5 (D-(−)-2-amino-5-phosphonopentanoic acid, an NMDA receptor antagonist), and DNQX (6,7-dinitroquinoxaline-2,3-dione, an AMPA/kainite receptor antagonist). For voltage clamp recordings, holding potential was −70mV; for current clamp recordings, resting potentials, after correction of liquid junction potential, ranged from −-72 to −-62 mV. Diffuse light stimuli, generated by the microscope's 100W tungsten-halogen lamp and transillumination optics, reached the retina through the coverslip forming the floor of the recording chamber using. The irradiance of the unattenuated stimulus (i.e. 0 log *I*) was 2.3×10^{13} photons cm^{-2} s^{-1} at the ganglion cell layer, sampled at 480 nm (see Wong et al. 2005 for methods). A logic-controlled shutter regulated stimulus timing. To visualize the morphology of recorded cells, they were filled through the patch pipette with Lucifer Yellow or Neurobiotin, fixed, processed (for Neurobiotin fills only) with Alexa 488-tagged streptavidin, and counterstained for melanopsin-like immunoreactivity (details about dye filling using sharp electrodes are found in supplementary experimental procedures).

Measuring acuity in the Visual Water Task

Apparatus and methodology were similar to that previously reported (Prusky et al., 2000). In brief, a trapezoidal-shaped pool was formed into a Y-maze by inclusion of a midline divider at the wide end. A computer monitor lay at the end of each arm, behind a glass wall. Water was added to the tank to a depth sufficient to submerge a platform, which was placed directly below the monitor displaying the positive (+; reinforced) stimulus. No platform was located below the monitor displaying the negative (−; non-reinforced) stimulus. Animals were trained to discriminate reliably between by swimming to the monitor displaying the reinforced stimulus and escaping the water by mounting the platform. The left/right position of the reinforced and non-reinforced stimuli were varied randomly except that the reinforced stimulus never remained in the same position for more than three trials. Trials were considered incorrect if animals swam beyond the end of the divider into the non-reinforced side of the maze. Visual stimuli were generated with, and experiments controlled by, custom software (Vista©, CerebralMechanics, Lethbridge, Canada) running on a G3 Apple Macintosh.

Grating acuity was measured by first training animals to discriminate a stationary, vertically-oriented sine wave grating (reinforced; maximum white=74 cd/m^2; minimum black=0.032 cd/m^2) from gray of the same mean luminance (non-reinforced; 43 cd/m^2). All light intensities were measured with a light meter from the position of the choice plane located at the end of the divider (Fig. 7B) where animals make their choices. We made sure that the luminance from the gray and sinusoidal screens are exactly the same (equiluminescent). The reason the mean is not half way between 74 and 0 cd/m^2 is the fact that 'black' is not 0 cd/m^2, due to the properties inherent to the monitor. Following training, the threshold to make the discrimination was determined by systematically increasing the spatial frequency of the reinforced stimulus over a series of interleaved trials until animals made fewer than 7 correct responses in a block of 10 trials, at least three times. For a grating of ~ 0.1 cycles/degree, 3 or 4 grating cycles were visible on the 17-inch monitor (We do not display partial cycles but only full cycles on the screen, i.e. when we increase the spatial frequency of the stimuli we do so by incrementally adding one cycle at a time. Thus, the stimuli vary only in spatial frequency). A minimum of 20 trials was run at each spatial frequency tested. A cumulative normal curve was fit to a plot of the data, and the point on the curve that intersected with 70% correct was adopted as the threshold. To measure the ability to make a discrimination

based on luminance (black vs. white), mice were trained as above to discriminate a monitor displaying black (reinforced; 0.032 cd/m^2) from a monitor displaying white (non-reinforced; 74 cd/m^2).

Measuring the spatial frequency threshold for optokinetic tracking

Apparatus and methodology were similar to that previously reported (Prusky et al., 2004). A vertical sine wave grating was projected as a virtual cylinder in 3D coordinate space on computer monitors surrounding a testing arena. We tested 9 different light intensities (54, 29, 15, 8, 4, 2.5, 2, 1.5, and 1 Lux) ranging from photopic all the way to scotopic light levels. Full details of this procedure are provided in the supplementary experimental procedures.

Pattern presentation induces cfos in the visual cortex

WT, *Gnat1*$^{-/-}$*; Cnga3*$^{-/-}$ (MO), and *Gnat1*$^{-/-}$*; Cnga3*$^{-/-}$*; Opn4*$^{-/-}$ (TKO) mice (n = 8,8,6) were housed in a 12:12 Light Dark cycle, and the experiment took place from ZT13-ZT16 for WT and MO animals (TKO animals free run and their circadian time was not determined for these experiments). Control mice (n=4,4,3) were removed from their home cage in the dark and placed in a 8.5”×8.5” room with black walls. Experimental (Pattern) mice (n=4,4,3) were placed in a room with the same dimensions but the walls had an alternating black and white bars (0.3” in width). Once in the room, a light (450 Lux) was turned on for 10 minutes. Following this, the light was turned off and the mouse was returned to its home cage. Eighty minutes later mice were deeply anesthetized with Avertin and perfused transcardially with 0.1M phosphate buffer followed by 4% PFA. Brains were removed and postfixed overnight in 4% PFA. After cryoprotection with 30% sucrose, brains were sectioned (40μm) through the rostro-caudal extent of V1 on a cryostat and processed immunohistochemically for cFos (see antibody staining in the supplementary experimental procedures).

Real Time quantitative PCR (qPCR)

RNA was extracted from retinas of WT and melanopsin-only mice using the RNeasy Mini Kit (QIAGEN). RETROscript kit (Ambion) was used to reverse transcribe poly(A) RNAs. Real-time qPCR was performed with iQ SYBR Green Supermix and iCycler iQ real-time PCR detection system (Bio-Rad). Each sample was analyzed in triplicate reactions of 50 μl. Primers for melanopsin are (Forward: GGGTTCTGAGAGTGAAGTGG, Reverse: AAGAGGCCTTGAGTTCTCC). Primers for our control (GAPDH) are (Forward: TTCACCACCATGGAGAAGGC, Reverse: GGCATGGACTGTGGTCATGA).

Supplementary Material

Refer to Web version on PubMed Central for supplementary material.

Acknowledgments

We would like to thank several people for providing reagents used in making the targeting construct: Naren Ramanan and David Ginty for the original Cre recombinase plasmid and FRT-flanked neomycin resistance cassette, and Jason Weil and Karen Beemon for the human beta-globin intron. The melanopsin antiserum was a kind gift from Ignacio Provencio. Z/AP mice were obtained from Tudor Badea in Jeremy Nathans laboratory who also provided lots of valuable discussions, and Z/EG mice from Seth Blackshaw. We also want to thank Dr. Rejji Kuruvilla, Dr. Haiqing Zhao and David McNeill for their careful reading of the manuscript and helpful suggestions and the Johns Hopkins University Mouse Tri-Lab for support. This work was supported by the National Institutes of Health grants GM076430 (S.H.), EY012793 (D.M.B.) and K99EY018863 (K.W.), the David and Lucile Packard Foundation (S.H.), and the Alfred P. Sloan Foundation (S.H.).

References

Altimus CM, Guler AD, Villa KL, McNeill DS, Legates TA, Hattar S. Rods-cones and melanopsin detect light and dark to modulate sleep independent of image formation. Proc Natl Acad Sci USA. 2008; 105:19998–20003. [PubMed: 19060203]

Badea TC, Nathans J. Quantitative analysis of neuronal morphologies in the mouse retina visualized by using a genetically directed reporter. J Comp Neurol. 2004; 480:331–351. [PubMed: 15558785]

Baver SB, Pickard GE, Sollars PJ. Two types of melanopsin retinal ganglion cell differentially innervate the hypothalamic suprachiasmatic nucleus and the olivary pretectal nucleus. Eur J Neurosci. 2008; 27:1763–1770. [PubMed: 18371076]

Berson DM, Castrucci AM, Provencio I. Morphology and mosaics of melanopsin-expressing retinal ganglion cell types in mice. J Comp Neurol. 2010; 518:2405–2422. [PubMed: 20503419]

Berson DM, Dunn FA, Takao M. Phototransduction by retinal ganglion cells that set the circadian clock. Science. 2002; 295:1070–1073. [PubMed: 11834835]

Biel M, Seeliger M, Pfeifer A, Kohler K, Gerstner A, Ludwig A, Jaissle G, Fauser S, Zrenner E, Hofmann F. Selective loss of cone function in mice lacking the cyclic nucleotide-gated channel CNG3. Proc Natl Acad Sci USA. 1999; 96:7553–7557. [PubMed: 10377453]

Calvert PD, Krasnoperova NV, Lyubarsky AL, Isayama T, Nicolo M, Kosaras B, Wong G, Gannon KS, Margolskee RF, Sidman RL, et al. Phototransduction in transgenic mice after targeted deletion of the rod transducin alpha -subunit. Proc Natl Acad Sci USA. 2000; 97:13913–13918. [PubMed: 11095744]

Cone RA. Early receptor potential: photoreversible charge displacement in rhodopsin. Science. 1967; 155:1128–1131. [PubMed: 6021913]

Coombs JL, Van Der List D, Chalupa LM. Morphological properties of mouse retinal ganglion cells during postnatal development. J Comp Neurol. 2007; 503:803–814. [PubMed: 17570502]

Dacey DM, Liao HW, Peterson BB, Robinson FR, Smith VC, Pokorny J, Yau KW, Gamlin PD. Melanopsin-expressing ganglion cells in primate retina signal colour and irradiance and project to the LGN. Nature. 2005; 433:749–754. [PubMed: 15716953]

Dkhissi-Benyahya O, Rieux C, Hut RA, Cooper HM. Immunohistochemical evidence of a melanopsin cone in human retina. Invest Ophthalmol Vis Sci. 2006; 47:1636–1641. [PubMed: 16565403]

Douglas RM, Alam NM, Silver BD, McGill TJ, Tschetter WW, Prusky GT. Independent visual threshold measurements in the two eyes of freely moving rats and mice using a virtual-reality optokinetic system. Vis Neurosci. 2005; 22:677–684. [PubMed: 16332278]

Gooley JJ, Lu J, Chou TC, Scammell TE, Saper CB. Melanopsin in cells of origin of the retinohypothalamic tract. Nat Neurosci. 2001; 4:1165. [PubMed: 11713469]

Guler AD, Altimus CM, Ecker JL, Hattar S. Multiple photoreceptors contribute to nonimage-forming visual functions predominantly through melanopsin-containing retinal ganglion cells. Cold Spring Harb Symp Quant Biol. 2007; 72:509–515. [PubMed: 18522518]

Guler AD, Ecker JL, Lall GS, Haq S, Altimus CM, Liao HW, Barnard AR, Cahill H, Badea TC, Zhao H, et al. Melanopsin cells are the principal conduits for rod-cone input to non-image-forming vision. Nature. 2008; 453:102–105. [PubMed: 18432195]

Hannibal J, Fahrenkrug J. Melanopsin containing retinal ganglion cells are light responsive from birth. Neuroreport. 2004; 15:2317–2320. [PubMed: 15640747]

Hatori M, Le H, Vollmers C, Keding SR, Tanaka N, Buch T, Waisman A, Schmedt C, Jegla T, Panda S. Inducible ablation of melanopsin-expressing retinal ganglion cells reveals their central role in non-image forming visual responses. PLoS ONE. 2008; 3:e2451. [PubMed: 18545654]

Hattar S, Kumar M, Park A, Tong P, Tung J, Yau KW, Berson DM. Central projections of melanopsin-expressing retinal ganglion cells in the mouse. J Comp Neurol. 2006; 497:326–349. [PubMed: 16736474]

Hattar S, Liao HW, Takao M, Berson DM, Yau KW. Melanopsin-containing retinal ganglion cells: architecture, projections, and intrinsic photosensitivity. Science. 2002; 295:1065–1070. [PubMed: 11834834]

Hattar S, Lucas RJ, Mrosovsky N, Thompson S, Douglas RH, Hankins MW, Lem J, Biel M, Hofmann F, Foster RG, Yau KW. Melanopsin and rod-cone photoreceptive systems account for all major accessory visual functions in mice. Nature. 2003; 424:76–81. [PubMed: 12808468]

Huberman AD, Manu M, Koch SM, Susman MW, Lutz AB, Ullian EM, Baccus SA, Barres BA. Architecture and activity-mediated refinement of axonal projections from a mosaic of genetically identified retinal ganglion cells. Neuron. 2008; 59:425–438. [PubMed: 18701068]

Huberman AD, Wei W, Elstrott J, Stafford BK, Feller MB, Barres BA. Genetic identification of an On-Off direction-selective retinal ganglion cell subtype reveals a layer-specific subcortical map of posterior motion. Neuron. 2009; 62:327–334. [PubMed: 19447089]

Kayama Y, Riso RR, Bartlett JR, Doty RW. Luxotonic responses of units in macaque striate cortex. J Neurophysiol. 1979; 42:1495–1517. [PubMed: 115968]

Kong JH, Fish DR, Rockhill RL, Masland RH. Diversity of ganglion cells in the mouse retina: unsupervised morphological classification and its limits. J Comp Neurol. 2005; 489:293–310. [PubMed: 16025455]

Lin B, Koizumi A, Tanaka N, Panda S, Masland RH. Restoration of visual function in retinal degeneration mice by ectopic expression of melanopsin. Proc Natl Acad Sci USA. 2008; 105:16009–16014. [PubMed: 18836071]

Livet J, Weissman TA, Kang H, Draft RW, Lu J, Bennis RA, Sanes JR, Lichtman JW. Transgenic strategies for combinatorial expression of fluorescent proteins in the nervous system. Nature. 2007; 450:56–62. [PubMed: 17972876]

Lobe CG, Koop KE, Kreppner W, Lomeli H, Gertsenstein M, Nagy A. Z/AP, a double reporter for cre-mediated recombination. Dev Biol. 1999; 208:281–292. [PubMed: 10191045]

Lucas RJ, Hattar S, Takao M, Berson DM, Foster RG, Yau KW. Diminished pupillary light reflex at high irradiances in melanopsin-knockout mice. Science. 2003; 299:245–247. [PubMed: 12522249]

Morin LP, Blanchard JH, Provencio I. Retinal ganglion cell projections to the hamster suprachiasmatic nucleus, intergeniculate leaflet, and visual midbrain: bifurcation and melanopsin immunoreactivity. J Comp Neurol. 2003; 465:401–416. [PubMed: 12966564]

Mrosovsky N, Hampton RR. Spatial responses to light in mice with severe retinal degeneration. Neurosci Lett. 1997; 222:204–206. [PubMed: 9148250]

Mrosovsky N, Salmon PA. Learned arbitrary responses to light in mice without rods or cones. Naturwissenschaften. 2002; 89:525–527. [PubMed: 12451457]

Novak A, Guo C, Yang W, Nagy A, Lobe CG. Z/EG, a double reporter mouse line that expresses enhanced green fluorescent protein upon Cre-mediated excision. Genesis. 2000; 28:147–155. [PubMed: 11105057]

Panda S, Sato TK, Castrucci AM, Rollag MD, DeGrip WJ, Hogenesch JB, Provencio I, Kay SA. Melanopsin (Opn4) requirement for normal light-induced circadian phase shifting. Science. 2002; 298:2213–2216. [PubMed: 12481141]

Prichard JR, Stoffel RT, Quimby DL, Obermeyer WH, Benca RM, Behan M. Fos immunoreactivity in rat subcortical visual shell in response to illuminance changes. Neuroscience. 2002; 114:781–793. [PubMed: 12220578]

Provencio I, Rodriguez IR, Jiang G, Hayes WP, Moreira EF, Rollag MD. A novel human opsin in the inner retina. J Neurosci. 2000; 20:600–605. [PubMed: 10632589]

Provencio I, Rollag MD, Castrucci AM. Photoreceptive net in the mammalian retina. This mesh of cells may explain how some blind mice can still tell day from night. Nature. 2002; 415:493. [PubMed: 11823848]

Prusky GT, Alam NM, Beekman S, Douglas RM. Rapid quantification of adult and developing mouse spatial vision using a virtual optomotor system. Invest Ophthalmol Vis Sci. 2004; 45:4611–4616. [PubMed: 15557474]

Prusky GT, Douglas RM. Characterization of mouse cortical spatial vision. Vision Res. 2004; 44:3411–3418. [PubMed: 15536009]

Prusky GT, West PW, Douglas RM. Behavioral assessment of visual acuity in mice and rats. Vision Res. 2000; 40:2201–2209. [PubMed: 10878281]

Quina LA, Pak W, Lanier J, Banwait P, Gratwick K, Liu Y, Velasquez T, O'Leary DD, Goulding M, Turner EE. Brn3a-expressing retinal ganglion cells project specifically to thalamocortical and collicular visual pathways. J Neurosci. 2005; 25:11595–11604. [PubMed: 16354917]

Reese BE. 'Hidden lamination' in the dorsal lateral geniculate nucleus: the functional organization of this thalamic region in the rat. Brain Res. 1988; 472:119–137. [PubMed: 3289687]

Robinson GA, Madison RD. Axotomized mouse retinal ganglion cells containing melanopsin show enhanced survival, but not enhanced axon regrowth into a peripheral nerve graft. Vision Res. 2004; 44:2667–2674. [PubMed: 15358062]

Ruby NF, Brennan TJ, Xie X, Cao V, Franken P, Heller HC, O'Hara BF. Role of melanopsin in circadian responses to light. Science. 2002; 298:2211–2213. [PubMed: 12481140]

Schmidt TM, Kofuji P. Functional and morphological differences among intrinsically photosensitive retinal ganglion cells. J Neurosci. 2009; 29:476–482. [PubMed: 19144848]

Schmidt TM, Taniguchi K, Kofuji P. Intrinsic and extrinsic light responses in melanopsin-expressing ganglion cells during mouse development. J Neurophysiol. 2008; 100:371–384. [PubMed: 18480363]

Sekaran S, Foster RG, Lucas RJ, Hankins MW. Calcium imaging reveals a network of intrinsically light-sensitive inner-retinal neurons. Curr Biol. 2003; 13:1290–1298. [PubMed: 12906788]

Sollars PJ, Smeraski CA, Kaufman JD, Ogilvie MD, Provencio I, Pickard GE. Melanopsin and non-melanopsin expressing retinal ganglion cells innervate the hypothalamic suprachiasmatic nucleus. Vis Neurosci. 2003; 20:601–610. [PubMed: 15088713]

Sun W, Li N, He S. Large-scale morphological survey of mouse retinal ganglion cells. J Comp Neurol. 2002; 451:115–126. [PubMed: 12209831]

Tu DC, Zhang D, Demas J, Slutsky EB, Provencio I, Holy TE, Van Gelder RN. Physiologic diversity and development of intrinsically photosensitive retinal ganglion cells. Neuron. 2005; 48:987–999. [PubMed: 16364902]

Viney TJ, Balint K, Hillier D, Siegert S, Boldogkoi Z, Enquist LW, Meister M, Cepko CL, Roska B. Local retinal circuits of melanopsin-containing ganglion cells identified by transsynaptic viral tracing. Curr Biol. 2007; 17:981–988. [PubMed: 17524644]

Volgyi B, Chheda S, Bloomfield SA. Tracer coupling patterns of the ganglion cell subtypes in the mouse retina. J Comp Neurol. 2009; 512:664–687. [PubMed: 19051243]

Wong KY, Dunn FA, Berson DM. Photoreceptor adaptation in intrinsically photosensitive retinal ganglion cells. Neuron. 2005; 48:1001–1010. [PubMed: 16364903]

Wong KY, Dunn FA, Graham DM, Berson DM. Synaptic influences on rat ganglion-cell photoreceptors. J Physiol. 2007; 582:279–296. [PubMed: 17510182]

Woodruff ML, Lem J, Fain GL. Early receptor current of wild-type and transducin knockout mice: photosensitivity and light-induced Ca2+ release. J Physiol. 2004; 557:821–828. [PubMed: 15073279]

Zaidi FH, Hull JT, Peirson SN, Wulff K, Aeschbach D, Gooley JJ, Brainard GC, Gregory-Evans K, Rizzo JF 3rd, Czeisler CA, et al. Short-wavelength light sensitivity of circadian, pupillary, and visual awareness in humans lacking an outer retina. Curr Biol. 2007; 17:2122–2128. [PubMed: 18082405]

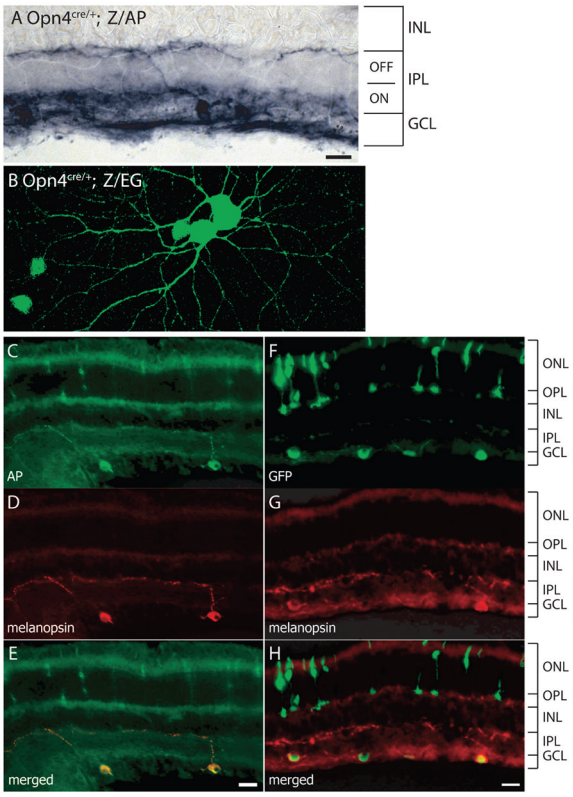

Fig. 1. Cre-mediated recombination with Z/AP and Z/EG reporters labels melanopsin-expressing ganglion cells

(A) Alkaline phosphatase staining of a vertical retinal section from an *Opn4*$^{Cre/+}$*; Z/AP* mouse reveals ganglion cells and their dendrites in both the ON and OFF sublaminae of the IPL. (B) *Opn4*$^{Cre/+}$*; Z/EG* retinal whole mount showing intrinsic GFP fluorescence signal in several retinal ganglion cells. (C–E) Double immunofluorescent labeling of ganglion cells with antibodies against alkaline phosphatase (C) and melanopsin (D). (F–H) Double immunolabeling of ganglion cells by antibodies against green fluorescent protein (F) and melanopsin (G). A few rod and cone cells labeled by the Cre reporter are visible in the ONL in C, E, F, and H, but these cells lack melanopsin immunoreactivity. ONL, outer nuclear layer; OPL, outer plexiform layer; INL, inner nuclear layer; IPL, inner plexiform layer; GCL, ganglion cell layer. Scale bars, 20 μm.

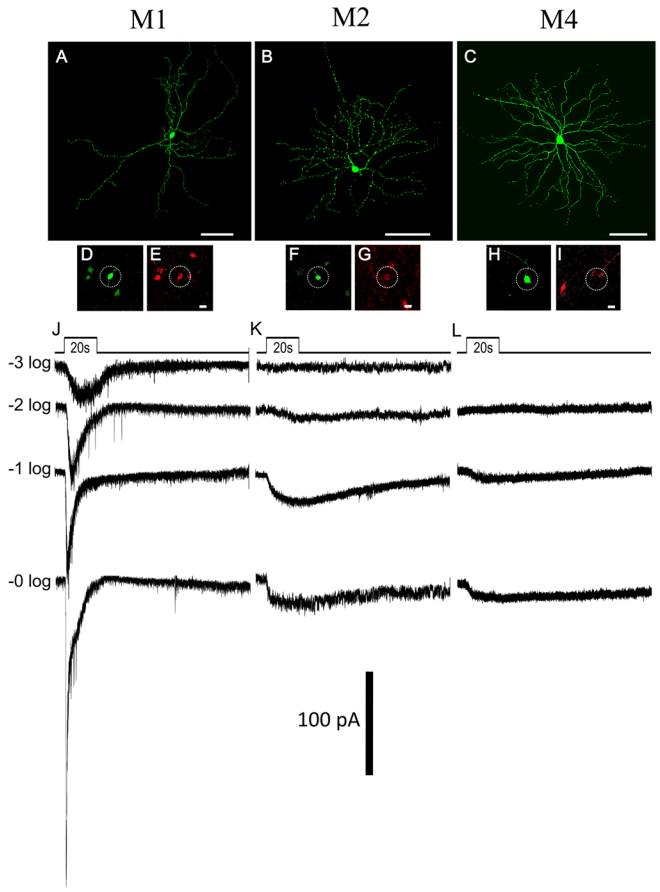

Fig. 2. Diversity of morphology and intrinsic light responses of ganglion cells GFP in the Opn4$^{Cre/+}$; Z/EG mouse

(A–C) Intracellular dye filling of representative examples of three subtypes of ipRGCs targeted by their GFP fluorescence in vitro, an M1 cell (A), an M2 cell (B), and an M4 cell (C). All three of these cells were intrinsically photosensitive, as shown by the whole cell voltage clamp recordings below (J, K, L), obtained during pharmacological blockade of retinal synapses. Light pulse was 20 seconds. Each trace in a given panel shows the response to a different light intensity. Values at left are the number of log units of attenuation in stimulus intensity from the maximal ("0 log"; 2.3×10^{13} photons cm^{-2} s^{-1}). Light-evoked currents were much larger in the M1 cell (J) than in the M2 cell (K) or M4 cell (L); they also returned more quickly to baseline after the stimulus. Fast downward deflections are presumed action currents resulting from incomplete voltage clamp. (D–I) Immunofluorescence (dotted circle) for melanopsin (E, G, and I) and Lucifer yellow injected cells (D, F, and H) show that M1 and M2 cells that are used for recording are melanopsin positive whereas the M4 cell (C, H, I and L) despite showing an intrinsic photoresponse lacked detectable melanopsin immunofluorescence. Note that this figure is optimized to highlight the recorded cells and hence some melanopsin positive cells appear to lack GFP labeling (more than 95% of melanopsin positive cells express GFP). Top trace in J slightly retouched to eliminate electrical artifact from series resistance test conducted well after the light response. Scale bars in A–C, 100 μm; D–I, 20 μm.

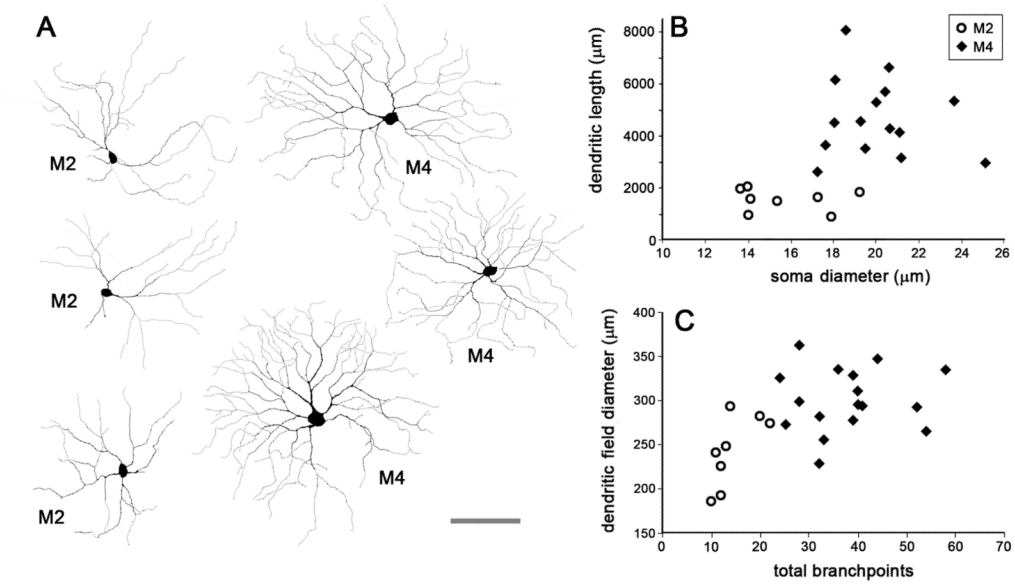

Fig. 3. Differences in soma size, dendritic field diameter, total branchpoints and dendritic length of M2 and M4 ipRGCs

(A) Six Lucida drawings of representative M2 and M4 ipRGCs. (B) Total dendritic branch length (TDBL) versus soma size of M2 and M4 cells (numbers are in μm, TDBL: M2; 1553 ± 428, M4; 4584 ± 1465, Soma Size: M2; 15.7 ± 2.2, M4 20.1 ± 2.2). (C) Dendritic field diameter versus total dendritic branchpoints of M2 and M4 cells (Total Branchpoints: M2; 14.3 ± 4.4, M4; 37.8 ± 9.6, Dendritic Field Diameter (μm): M2; 243 ± 39.9, M4; 301 ± 35.4). Open circles are M2 ipRGCs while black diamonds are M4 ipRGCs. Range is provided as average ± standard deviation.

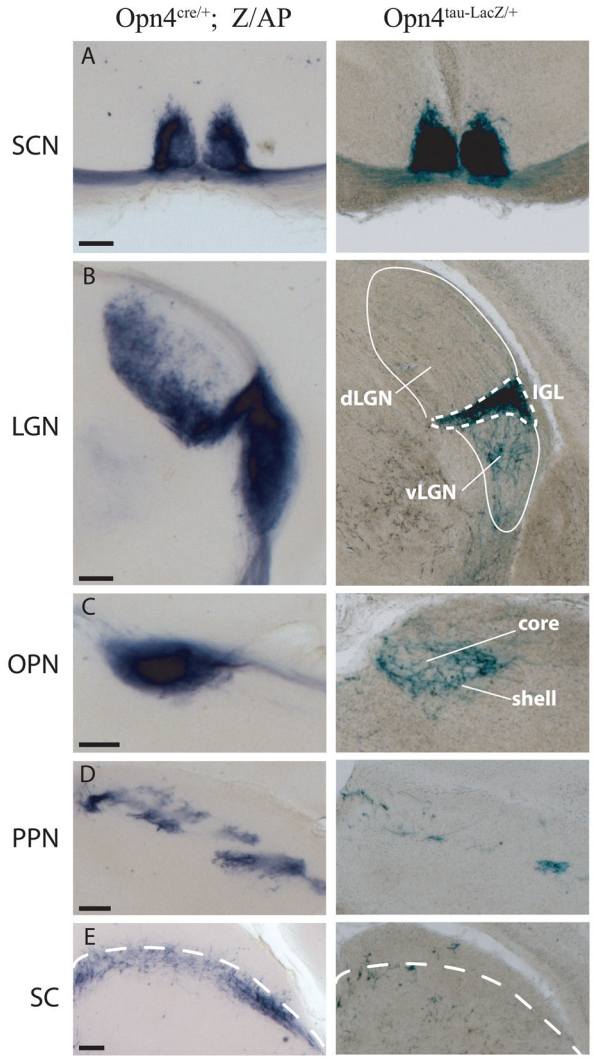

Fig. 4. Comparison of retinofugal projections of presumed melanopsin-expressing ganglion cells as revealed by two lines of reporter mice in representative coronal sections

Left column: axons of ipRGCs revealed by alkaline phosphatase histochemical labeling in *Opn4*$^{Cre/+}$*; Z/AP* mice. *Right column*: axons of a subset of M1 melanopsin ganglion cells by X-gal staining in *Opn4*$^{tau\text{-}LacZ/+}$ mice. (A) The suprachiasmatic nucleus (SCN), (B) Lateral geniculate nucleus (LGN), showing the intergeniculate leaflet (IGL, dotted lines) flanked by the dorsal LGN (dLGN, upper solid white outline) and ventral LGN (vLGN, lower solid white outline). Labeling of the dLGN and vLGN is much more prominent in *Opn4*$^{Cre/+}$*; Z/AP* sections (left). (C) Olivary pretectal nucleus (OPN). Whereas fiber labeling is largely restricted to the shell of the nucleus in *Opn4*$^{tau\text{-}LacZ/+}$ mice (right), the core of the nucleus is also strongly labeled in the *Opn4*$^{Cre/+}$*; Z/AP* model (left). (D) The posterior pretectal nucleus (PPN) contains minimal fiber labeling in *Opn4*$^{tau\text{-}LacZ/+}$ brains, but exhibits strong, patchy labeling in the *Opn4*$^{Cre/+}$*; Z/AP* mouse. (E) The superior colliculus (SC) contains only a few labeled fibers in the *Opn4*$^{tau\text{-}LacZ/+}$ mouse, but much more extensive labeling in the *Opn4*$^{Cre/+}$*; Z/AP* animal, especially in the stratum opticum. Dotted line marks approximate boundary between the superficial gray layer and stratum opticum. Scale bars, 200 μm.

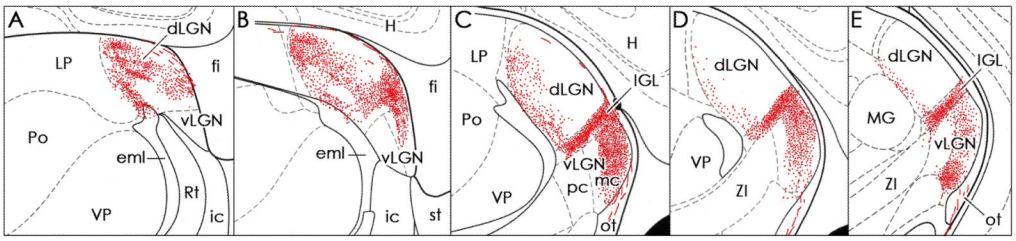

Fig. 5. Charting of the synaptic input from ipRGCs to the LGN complex

Charting of alkaline-phosphatase positive retinal fibers in the lateral geniculate nucleus, as seen at five coronal levels, shows substantial innervation of the dLGN from ipRGCs. The section in A is most rostral, E most caudal. Abbreviations: dLGN, dorsal lateral geniculate; eml, external medullary lamina; fi, fimbria; H, hippocampus; ic, internal capsule; IGL, intergeniculate leaflet; LP, lateral posterior nucleus; MG, medial geniculate nucleus; ot, optic tract; Po, posterior nuclei; Rt, thalamic reticular nucleus; st, stria terminalis; vLGN, ventral lateral geniculate (including parvocellular [pc] and magnocellular [mc] subdivisions); VP, ventral posterior nucleus; ZI, zona incerta.

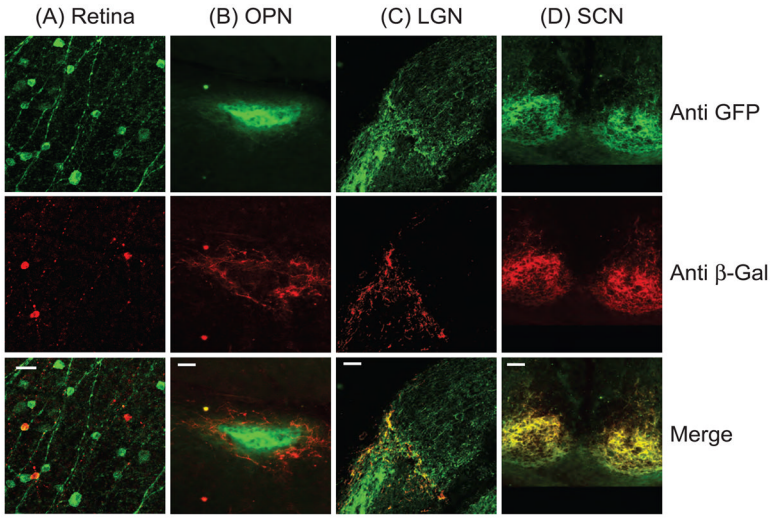

Fig. 6. Direct comparison in *Opn4*$^{Cre/tau\text{-}LacZ}$; *Thy-1-Brainbow-1.0* mice labeling of retinal neurons and retinofugal axons by the two reporters of melanopsin expression

Anti-β-galactosidase immunoreactivity (red fluorescence) marks M1 ipRGCs and axons; GFP-like immunofluorescence (green) labels fluorescent proteins expressed in all subtypes of ipRGCs. (A) Retinal whole mount. Antibody labeling reveals that the Cre-mediated reporter (green) is present in most β-galactosidase immunoreactive cells (red) but is much more widely expressed. (B–D) Fiber labeling in selected coronal brain sections. In the olivary pretectal nucleus (B), M1 axons, expressing β-galactosidase (red) are largely restricted to the shell of the nucleus, whereas the fluorescent proteins (green) heavily label axons in the core as well as more weakly double-labeling the β-gal-positive axons in the shell. In the LGN (C), the intergeniculate leaflet contains a mixture of double-labeled axons (yellow; M1 afferents) and axons labeled only with fluorescent proteins (green; presumably from M2, M4 and/or M5 ipRGCs). The latter are also visible in parts of the vLGN and in the dLGN. (D) The suprachiasmatic nucleus (SCN) contains mainly double labeled fibers, indicating that most retinal afferents originate in M1 cells, though at higher magnification some fibers singly labeled for fluorescent proteins (green) can be seen (not shown).

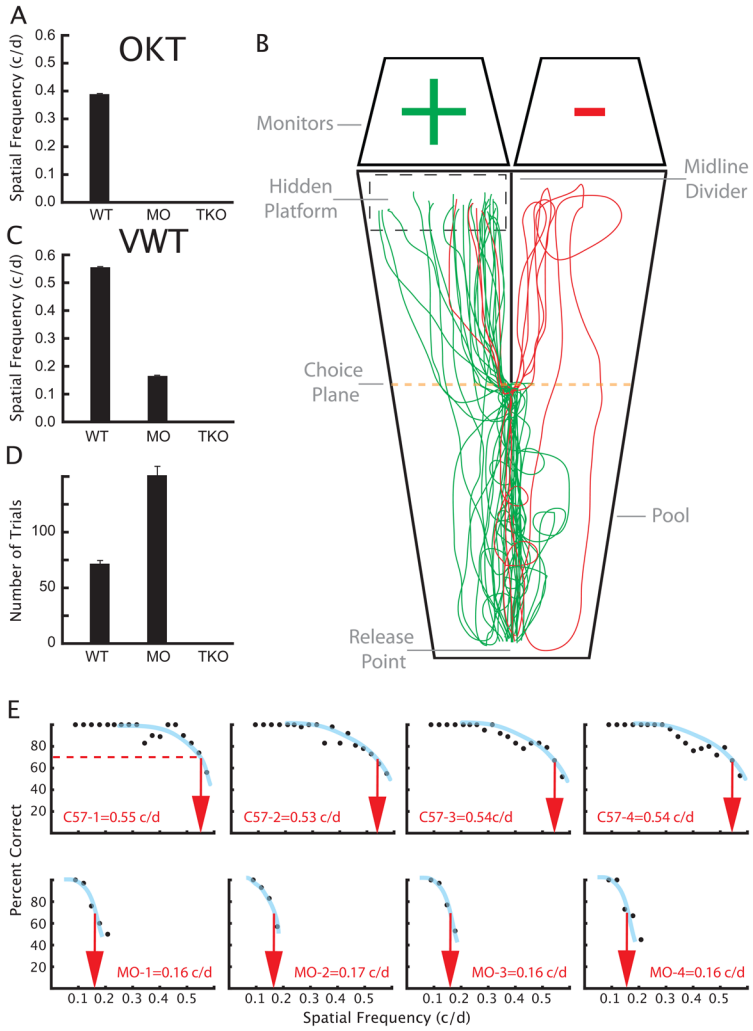

Fig. 7. Mice in which ipRGCs are the sole functional photoreceptor (*Gnat1*$^{-/-}$; *Cnga3*$^{-/-}$ animals, MO: "melanopsin only" animals) can discriminate patterns

(A) Optokinetic tracking (OKT). Spatial frequency threshold for in C57/Bl6 mice (WT, n = 5; 0.392 c/d (SEM=0.001)) was comparable to previously reported values (C57 mice (n = 7); 0.397 c/d (SEM=0.001)), but no tracking was observed at any spatial frequency in *Gnat1*$^{-/-}$; *Cnga3*$^{-/-}$ mice or in mice lacking any functional photoreceptors (triple knockouts *Gnat1*$^{-/-}$; *Cnga3*$^{-/-}$; *Opn4*$^{-/-}$; TKO). (B) Individual movement trajectories of an *Gnat1*$^{-/-}$; *Cnga3*$^{-/-}$ (MO) animal performing the Visual Water Task (VWT). Green trajectories indicate successful attempts to locate the platform under the monitor displaying the grating (+); red trajectories are failures. (C) Spatial frequency thresholds (acuity) measured in the Visual Water Task. Acuity of C57/Bl6 mice (WT, n = 5; 0.55 c/d (SEM=0.006)) was similar to previously reported values (C57 mice (n = 7); 0.54 c/d (SEM=0.0005)). Acuity of *Gnat1*$^{-/-}$; *Cnga3*$^{-/-}$ animals was lower but measurable at (0.16 c/d (SEM=0.002); n = 9). Triple knockout animals (n = 7) could not perform the task, so no threshold could be obtained. (D) Mean number of trials required to reach criterion performance in the Visual Water Task on a discrimination between a sine wave grating (0.12 c/d) and uniform gray of the same mean luminance. Wildtype mice (C57/Bl6; n = 5) averaged 71 (SEM=2.4) trials to achieve criterion performance, while *Gnat1*$^{-/-}$; *Cnga3*$^{-/-}$ mice (n = 9) reached the criterion in an average of 148 (SEM=9.2) trails. The triple knockout animals (n = 7) failed to reach criterion in 405 trials. (E) Raw performance as a function of spatial frequencies for four

individual C57 wildtype and *Gnat1*$^{-/-}$*; Cnga3*$^{-/-}$ animals. Error bars in A, C and D are standard error of the mean.

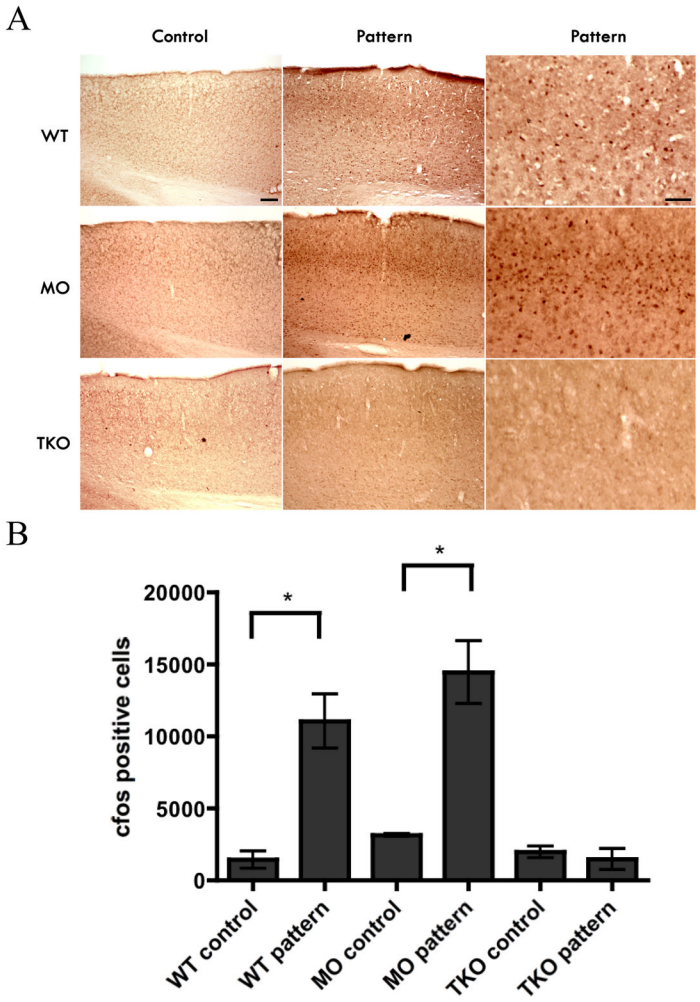

Fig. 8. Pattern induced activation of cfos in the visual cortex in WT and *Gnat1*$^{-/-}$; *Cnga3*$^{-/-}$ mice, but not in triple knockout animals

(A) Fos positive cells were observed in the V1 region of the visual cortex in WT and *Gnat1*$^{-/-}$; *Cnga3*$^{-/-}$ (MO) mice that were exposed to a pattern for ten minutes under a 450 lux white light (Pattern), but not in animals exposed to the same light intensity without a pattern (Control). Fos positive cells were not observed in triple knockout (TKO) mice exposed to either condition. Panels to the right are magnification of each cortical region showing either lack or presence of nuclear cfos staining. (B) Quantification of the data by counting the number of cfos positive cells in V1. Note that only WT and MO animals show significant increases compared to control levels. Statistical analysis was carried out using unpaired student's t-test.